PAPER • OPEN ACCESS

Power performance of a model floating wind turbine subjected to cyclic pitch motion: A wind tunnel study

View the article online for updates and enhancements.

Power performance of a model floating wind turbine subjected to cyclic pitch motion: A wind tunnel study

Guiyue Duan[1], Daniele Gattari[1] and Fernando Porté-Agel[1]

[1]Wind Engineering and Renewable Energy Laboratory (WIRE), École Polytechnique Fédérale de Lausanne (EPFL), 1015 Lausanne, Switzerland

E-mail: `guiyue.duan@epfl.ch` (Guiyue Duan)

Abstract. Wind tunnel experiments were performed with a miniature floating wind turbine model to study the effects of cyclic pitch motion on its power performance. The cyclic pitch motion was prescribed by two key parameters: pitch frequency and amplitude. The power performance of the turbine model was investigated at a frequency range of $0.1 - 5.0 Hz$ and an amplitude range of $0 - 30°$. Both the mean and time variation of the power production were analyzed, and the effects of the pitch parameters, i.e., the pitch amplitude and frequency, were investigated and discussed. The results show a clear periodicity of power variation and its dependence on pitch frequency and amplitude. For relatively small pitch frequencies $(0.5 - 3.0 Hz)$, the mean power and periodic power variation can be predicted based on the uniform and steady flow assumption. Compared to the power output in the baseline case of no pitch dynamics, cyclic pitch motions were found to cause higher power fluctuations, which were contributed by both the pitch motion and flow turbulence. Finally, the temporal variation of the free-rotation speed, used as an indicator of available aerodynamic power, is found to be periodic when the turbine is under cyclic pitch motion. This suggests the possibility of applying dynamic rotor control strategies to maximize power production.

1. Introduction

Offshore floating wind turbines (OFWTs) are becoming increasingly popular due to their ability to exploit deep-sea wind resources [1]. However, since wind turbines are installed on floaters instead of solid foundations, the dynamic response of an OFWT due to the wind-wave-structure coupled effects [2] can bring structure safety concerns [3] and affect the power performance [4]. Different concepts of floaters [5], such as spar-type and semi-submersible floaters have been developed in order to ensure the safe operation of OFWTs in various ocean states. These floaters are designed with damping mechanism and mooring system to prevent large-amplitude dynamic response. However, due to their floating nature, the dynamic response of OFWTs in an environment with external excitation (e.g., waves) cannot be completely suppressed. Therefore, it is essential to understand the impacts of dynamic response on the performance of OFWTs.

The dynamic response of an OFWT can be described by motions in six different degrees of freedom (DOFs) or directions, which are surge, sway, heave, roll, pitch and yaw, as illustrated in Figure 1(a). Among the six DOFs, the two most pronounced motions are surge motion and pitch motion, which are the fore-and-aft translation and rotation, respectively. However, when focusing on the motion of the rotor plane, the kinematics in pitch motion are more complex than surge motion. This is because, during the pitch motion, the rotor plane undergoes not

only the out-of-plane rotation (i.e., the variation of the tilt angle) but also has two translational velocity components in the heave and surge motion directions (although these can be small when pitch dynamics are not very strong), respectively. During the pitch motion, as the pitch angle changes, the motion-induced out-of-plane rotor velocity varies continuously, and so does the inflow condition because the closer to the surface, the lower the streamwise inflow velocity (see Figure 1(b)) and the higher the turbulence intensity. Different from the single DOF out-of-plane rotation situation, for example, the cyclic yaw motion, whose rotation center can be considered as fixed [6], the pitch-induced rotor velocity depends on not only the pitch frequency and pitch amplitude but also the pitch rotation radius (e.g., the tower height). In addition, considering the aerodynamics of a rotor in cyclic pitch motion, the kinematics of a blade element in dynamic motion can be very different from the static turbine case: the motion-induced velocity and acceleration can affect the lift and drag exerted on the blade element, which consequently affects the power performance of the turbine.
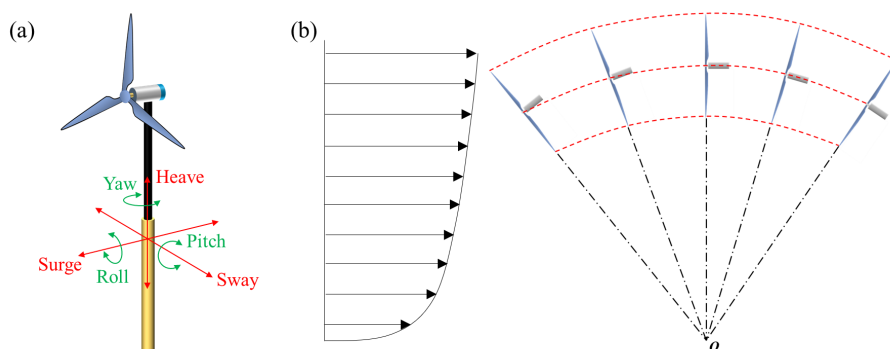
Figure 1. (a) 6 degrees of freedom in the dynamic motion of an OFWT and (b) motion of the rotor plane of an OFWT during dynamic pitch response. O is the center of the pitch rotation.

In the current study, based on wind tunnel experiments and a miniature wind turbine model, the effects of dynamic pitch motion on power performance are investigated. For simplicity and feasibility, only the cyclic pitch motion is considered and the motion is imposed from an in-house developed pitching platform. The rest of the paper is structured as follows: section 2 introduces the details of experimental setup and measurements; section 3 presents the power results and analysis; the summary and future perspectives are presented in section 4.

2. Setup and method

Wind tunnel experiments were performed with a model wind turbine mounted on a pitch motion platform developed in-house, as presented in Figure 2. In reality, pitch motion of an OFWT can be regular or irregular, or even coupled with other motions in different DOFs, due to the complex wind-wave-structure interactions. For simplicity, the cyclic (i.e., sinusoidal) pitch motion of the OFWT model was studied in the present work. The two main control parameters are the pitch frequency (f) and the pitch amplitude (θ_{max}, i.e., maximum pitch angle). The equation of pitch angle θ at a given time t can be written as

$$\theta(t) = \theta_{max} \sin(2\pi f t). \tag{1}$$

The range of control parameters that can be tested in the current setup is limited by the maximum torque of the pitch platform. Table 1 shows the values of the control parameters used in this study.

Table 1. Control parameters that can be tested for power measurements.

Pitch amplitude $\theta_{max}(°)$	Pitch frequency range $f(Hz)$
5	0-5
10	0-4
15	0-3
20	0-2
25	0-0.5
30	0-0.1
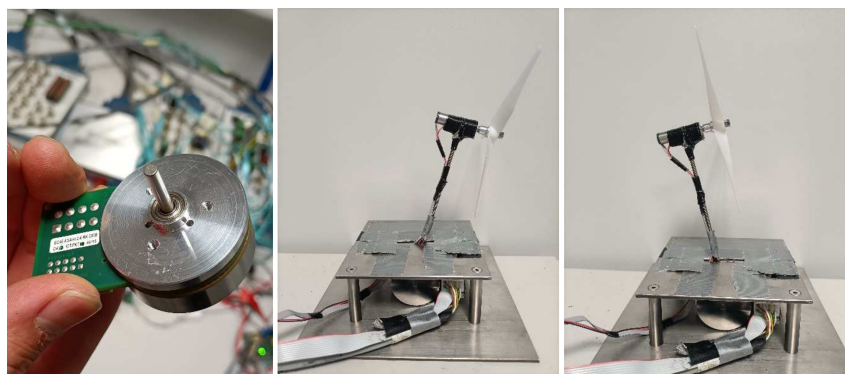
Figure 2. The in-house developed pitch platform with the WiRE-01 miniature wind turbine. From left to right are: the Maxon EC-flat motor, the turbine model in forward pitch and the turbine model in backward pitch.

Experiments were conducted in a close-loop atmospheric boundary layer wind tunnel, whose test section is 28m long, 2.6m wide and 2.0m high. The wind turbine model used in this study is the WiRE-01 miniature wind turbine which has a rotor diameter of 0.15m and a hub height of 0.125m. The power extracted was measured by the generated electric power, with the shaft friction loss and electromagnetic loss calibrated [7]. It is worth mentioning that the WiRE-01 miniature wind turbine has a thrust coefficient of around 0.8 and a power coefficient of around 0.4 [7], which are close to those of large-scale wind turbines. To test the OFWT model in a boundary layer flow, the pitch-driven platform was placed under the floor and the inflow boundary layer was naturally developed along the test section without using additional tripping mechanisms. The vertical profiles of the inflow at the test position are shown in Figure 3. At the hub-height level, the streamwise velocity is $\overline{u}_{hub} \approx 4.0m/s$ and the streamwise turbulence intensity ($\sigma_u/\overline{u}_{hub}$, where σ_u is the standard deviation of hub-height streamwise velocity) is around 0.07. For each selected combination of control parameters, power measurements were conducted at a sampling frequency of 1000Hz for 180s.

3. Results and discussion
To better understand the effects of cyclic pitch motion on the power performance of an OFWT, the time variation of power production, the average power output and the power fluctuations are analyzed. Some results are also compared with the fixed pitch (i.e., tilt) cases to show the effects of the dynamic motion.

3.1. Time variation of the instantaneous power output
The time variation of the normalized power outputs (P/P_m^{base}, where P is the instantaneous power and P_m^{base} is the mean power of the baseline case) in an arbitrarily selected time interval
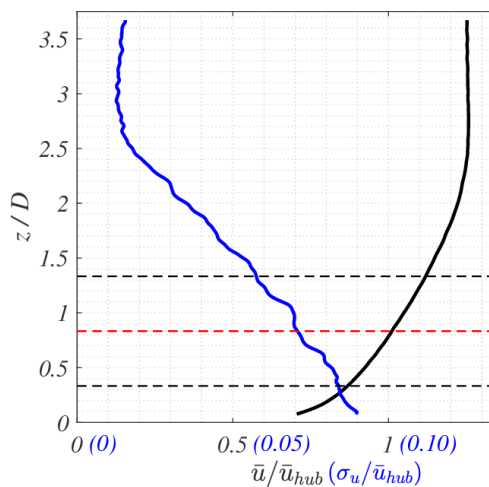
Figure 3. Vertical inflow profiles of the normalized mean streamwise velocity and the streamwise turbulence intensity. The dashed red line denotes the hub height and the dashed black lines denote the upper and lower rotor edges.

comprising two pitch cycles are presented in Figure 4. It is found that at low pitch frequencies, e.g., Figure 4(a) power fluctuations are comparable to the baseline case, even in cases with relatively high pitch amplitudes. Meanwhile, for small pitch amplitudes, e.g., Figure 4(b), the range of power variation are quite similar to the baseline case). This is because the pitch frequency or amplitude is so small that the dynamic effects on power output can be ignored. The dynamic effects can be related to the motion-induced velocity on the rotor plane. Based on Equation (1), the pitch-induced velocity u_p at the rotor center can be written as

$$u_p(t) = h \cdot \dot{\theta}(t) = 2\pi f h \theta_{max} \cos(2\pi f t), \tag{2}$$

where h is the pitch rotation radius or turbine hub height. For very small pitch frequencies (f) or amplitudes (θ_{max}), $\|u_p\| \leq 2\pi h f \theta_{\max} \ll \overline{u}_{hub}$ (similar when considering the motion-induced acceleration), the effects of pitch dynamics can be reasonably ignored.

For cases with higher pitch frequencies, power output variations are more regular, i.e., periodic, and the maximum and minimum power outputs are found to be dependent on the pitch amplitude. Figure 5 presents the power spectral density (PSD) of power signals in different cases. It can be seen that power signals are less periodic in cases with $f = 0.1Hz$, compared to those cases with higher frequencies (which show dominant frequencies that are the same as their motion frequencies). The magnitude of PSD (i.e., energy) corresponding to the peak frequency increases with the increase of pitch amplitude, which implies an increasing periodicity in power variation. Mathematically speaking, the standard deviation of a given sine function only depends on the amplitude. Therefore, if we assume that the power variation of an OFWT under cyclic pitch motion approximately follows a sine function, the standard deviation can be divided into two parts: (1) the part contributed by the periodic variation, which only depends on the amplitude of the function; (2) the contribution from non-periodic power fluctuations, which can be computed based on the differences between the real-time power production and periodic variation.

3.2. The mean and standard deviation of power outputs
To evaluate the effects of dynamic pitch, power results of the fixed pitch situation are also studied. According to Bastankhah and Porté-Agel [8], for the WiRE-01 miniature wind turbine,
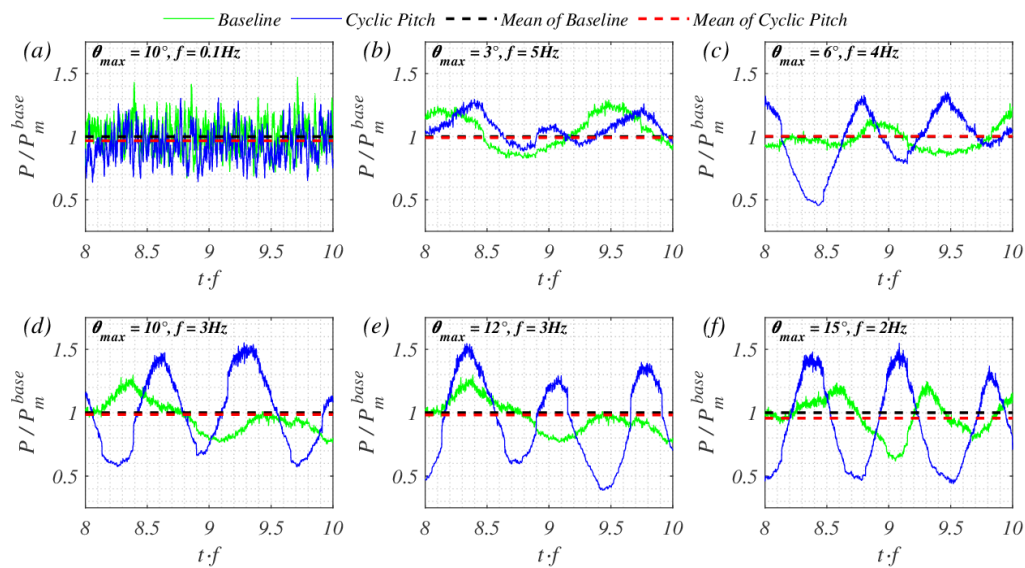
Figure 4. Normalized power production of the OFWT model as a function of the normalized time ($t \cdot f$, where t is the time and f is the pitch frequency) during different prescribed cyclic pitch motions.
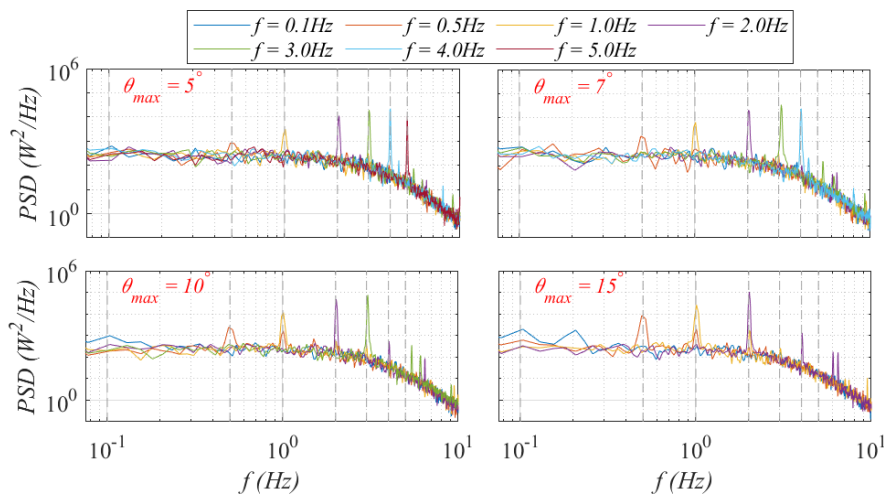

Figure 5. Power spectral density (PSD) of the OFWT model power outputs in different combinations of f and θ_{max}.

the normalized mean power production (P_m/P_m^{base}, where P_m is the mean power) of a turbine at a yaw angle of γ follows well the $\cos^3(\gamma)$ relation. However, as presented in Figure 6(a), differences are found in the fixed pitch situation: for backward pitch P_m/P_m^{base} lies between $\cos(\theta)$ and $\cos^2(\theta)$; while for forward pitch P_m/P_m^{base} lies between $\cos^3(\theta)$ and $\cos^4(\theta)$. In addition, power production in the backward pitch case at $\theta = 5°$ is found to be slightly larger than in the baseline case. These are because, for the lab-scale WiRE-01 turbine used in this study, the overhang is around 20% of the rotor diameter, leading to a higher hub height in backward pitch than in forward pitch of the same pitch angle (and a slightly higher hub height than in the baseline case when in backward pitch at $\theta = 5°$). For utility-scale wind turbines, the

impacts of overhang are usually negligible as it is much smaller (e.g., 4% of the rotor diameter for the NREL 5MW wind turbine). For wind-tunnel experiments, especially in a boundary layer flow of high shear, it might be necessary to consider the effect of the overhang. Compared to fixed pitch cases, P_m/P_m^{base} for most of the cyclic pitch cases lies between $\cos(\theta)$ and $\cos^2(\theta)$, depending on the pitch frequency and amplitude, as shown in Figure 6(a). In general, within the frequency range tested, the mean power production increases with the increasing frequency.

It is also found that the standard deviation of the power output (σ_P) is higher in cyclic pitch cases but lower in fixed pitch cases, compared with the baseline case. As shown in Figure 6(b), for fixed pitch cases the normalized standard deviation (σ_P/P_m^{base}) can be less than in the baseline case at high pitch angles due to lower power production, while the values of σ_P/P_m lie in the range of $0.11-0.14$, close to the value of 0.12 in the baseline case. In the cyclic pitch cases, the standard deviation increases with the increase of both the pitch angle amplitude and the pitch frequency. It is worth noting that the periodic power variation caused solely by the cyclic pitch motion is also treated as fluctuations when calculating the standard deviation. As previously mentioned, if the periodic power variation can be expressed as a sine function, the standard deviation then could be considered contributed from both the cyclic motion and the inflow turbulence.
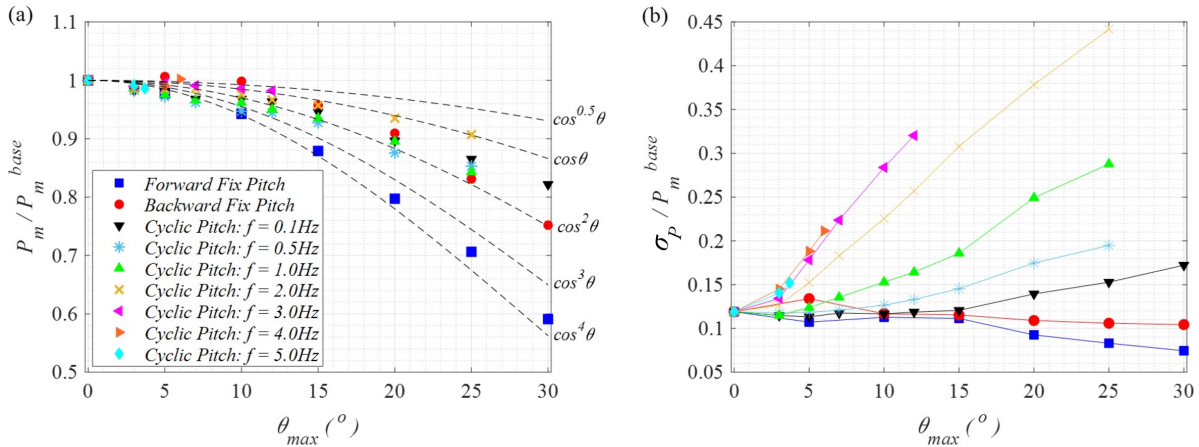
Figure 6. Normalized (a) mean and (b) standard deviation of power outputs as functions of pitch frequency and pitch amplitude.

For a periodic power variation, the instantaneous power P at time t can be decomposed into the mean power P_m, the periodic power variation $\widetilde{P}(t)$ and the fluctuation part $P'(t)$, which can be written as

$$P(t) = P_m + \widetilde{P}(t) + P'(t). \tag{3}$$

Notice that $\int_0^T \widetilde{P}(t)\,dt = 0$ and $\int_0^T P'(t)\,dt = 0$, where T is the period of cyclic pitch motion. To obtain P_m and $\widetilde{P}(t)$, the uniform flow assumption is applied and the hub-height velocity is used as a representative velocity. During the cyclic pitch motion, the relative velocity perpendicular to the rotor plane is given as

$$u(t) = \overline{u}_{hub} \cdot \cos(\theta(t)) + h \cdot \dot{\theta}(t) + u'(t), \tag{4}$$

where $u'(t)$ is considered as the velocity fluctuation. If assuming the flow is steady, which leads to $u'(t) = 0$, and considering only small pitch amplitudes (i.e., $\theta_{max} \leq 15°$), we can obtain

$$\frac{P_m}{P_m^{base}} \cdot \frac{C_P^{base}}{C_P} \approx 1 + \frac{3s^2}{2}, \tag{5}$$

where $C_P = 2P/\left(\rho A u^3\right)$ is the power coefficient (ρ is the air density and A is the rotor-swept area) and $s = 2\pi f h \theta_{max}/\overline{u}_{hub}$ is the ratio between the maximum pitch-induced velocity and the inflow velocity. Following same assumptions of steady uniform flow and small pitch amplitude, as mentioned previously, we can obtain

$$\frac{\widetilde{P}(t)}{P_m^{base}} \cdot \frac{C_P^{base}}{C_P} \approx 3s \cdot \cos\left(2\pi ft\right) + \frac{3s^2 \cdot \cos\left(4\pi ft\right)}{2} + s^3 \cdot \cos^3\left(2\pi ft\right). \tag{6}$$

According to Equation (6), $\widetilde{P}(t)$ varies periodically with t, with an upper bound

$$\widetilde{P}_{up} = \left(3s + \frac{3s^2}{2} + s^3\right) \frac{C_P}{C_P^{base}} P_m^{base}, \tag{7}$$

and a lower bound

$$\widetilde{P}_{low} = \left(-3s + \frac{3s^2}{2} - s^3\right) \frac{C_P}{C_P^{base}} P_m^{base}. \tag{8}$$

If $C_P \approx C_P^{base}$, which can be applicable if the motion amplitude is small,

$$\widetilde{P} \in \left[-3s + \frac{3s^2}{2} - s^3,\ 3s + \frac{3s^2}{2} + s^3\right]. \tag{9}$$

It should be noted that if $C_P \approx C_P^{base}$ stands, the cyclic pitch cases should always produce more power than the baseline case, according to Equation (5). However, based on the results shown in Figure 6(a), the mean power production decreases when θ_{max} increases. This indicates that C_P itself is a function of θ_{max} and f, which can be attributed to the fact that rotor aerodynamics are different in the dynamic pitch situation. For example, C_P might decrease when dynamic stall occurs or when the resultant velocity at the rotor is too small during backward pitch (i.e., Reynolds number effect). For example, C_P might decrease when dynamic stall occurs. Besides, C_P may also decrease when the resultant velocity at the rotor is too small during backward pitch, resulting in a lower C_P due to worse aerodynamics (e.g., a lower lift coefficient) at lower Reynolds numbers [7].

Comparisons between the average upper bound of $\widetilde{P}(t)$ (i.e., $\widetilde{P}_{up}$) based on the measured power data and the bound predicted by Equation (7) for various cases are presented in Figure 7(a). It is found that $\widetilde{P}_{up}$ can be acceptably estimated for $0.5Hz \leq f < 3.0Hz$. For $f = 0.1Hz$, the impacts of pitch motion are negligible compared to the impacts caused by flow turbulence; while for $f \geq 3.0Hz$ the pitch dynamics become significant so that the assumptions applied to Equation (6) cannot hold. According to Equation (3), the real-time power fluctuations can be given by $P(t) - P_m = \widetilde{P}(t) + P'(t)$, the standard deviation of power production, σ_P, can thus be written as

$$\sigma_P = \sqrt{\frac{1}{T}\int_0^T \left[\widetilde{P}(t)\right]^2 \mathrm{d}\,t + \frac{1}{T}\int_0^T \left[P'(t)\right]^2 \mathrm{d}\,t}, \tag{10}$$

which includes the contribution from the periodic power variation $\widetilde{P}(t)$ and the non-periodic part $P'(t)$ (assuming that $\widetilde{P}(t)$ and $P'(t)$ are uncorrelated). If separating the contribution by $\widetilde{P}(t)$, which can be obtained based on Equation (6), the contribution from $P'(t)$, σ'_P, can be written as

$$\sigma'_P = \sqrt{\sigma_P^2 - \left(4.5s^2 + 3.375s^4 + 0.3125s^6\right) \cdot \left(\frac{C_P}{C_P^{base}} P_m^{base}\right)^2}. \tag{11}$$

Assuming $C_P \approx C_P^{base}$, σ_P' can be calculated based on Equation (6). Figure 7(b) presents σ_P'/P_m^{base} as a function of θ_{max} at different pitch frequencies. For cases with relatively small θ_{max} and f values, σ_P' is very close to that of the baseline case. It is interesting to see that σ_P' is much smaller compared to σ_P (see in Figure 6(b)). The difference in σ_P' between the baseline case and cyclic pitch cases might be related to the flow-structure interactions during the pitch motion, i.e., the fact that flow around the rotor can also be affected by the pitch motion.
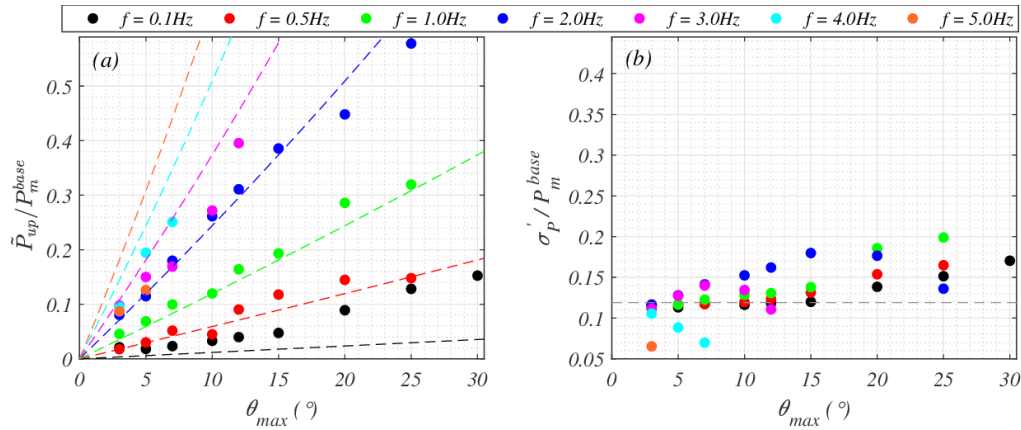

Figure 7. (a) The upper bound of periodic power variation, $\widetilde{P}_{up}$, normalized by P_m^{base}. The dashed lines are the results predicted based on Equation (10). (b) Normalized power standard deviation subtracting the contribution from periodic variation, based on Equation (11). The gray dashed line represents the power standard deviation in the baseline case.

### 3.3. Turbine as a sensor of available aerodynamic power

When let rotate freely, the wind turbine itself can act as a sensor of the wind speed or wind power, which can be used as an effective indicator of the power that can be extracted by the turbine. Figure 8(a) shows the variation of the mean free-rotation rotor speed (Ω_f) with different fixed pitch angles, i.e., different tilt angles (β). The asymmetry between forward pitch and backward pitch cases is due to the asymmetry in the hub height and, thus, the hub-height inflow velocity, caused by the existence of overhang. This free-rotation speed can be further used to quantify the optimal rotor speed for maximum power production [9]. Figure 8(b) shows the optimal rotation speed, Ω_{opt} (corresponding to the maximum power production) as a function of the free-rotation speed, Ω_f, measured by fixing the turbine model at different pitch angles, i.e., different tilt angles. It can be seen that there is a clear linear relation between the Ω_f and Ω_{opt}. It is worth noting that to obtain the results presented in Figure 8(b), there is no necessity to know the value of β: the turbine will run faster in free-rotation response when the wind power (i.e., the available aerodynamic power) is higher.

When the OFWT model is subjected to cyclic pitch motion, the temporal variation of free-rotation speed (e.g., shown in Figure 9) is periodic and dependent on the pitch parameters, i.e., pitch amplitude and frequency. This suggests that a cyclic rotor speed control could be helpful to dynamically track the maximum power points. For lab-scale wind turbines, this requires the knowledge of optimal rotor speed variations during cyclic pitch motions, which can be obtained from free-rotation response tests. Assuming $\Omega_f = \Omega_f(u_{hub}, \theta)$, based on Taylor expansion, the free-rotation speed can be approximated by

$$\Omega_f \approx \Omega_{f,0} + \partial_u \Omega_{f,0} h \dot{\theta} + \partial_\theta \Omega_{f,0} \theta = \Omega_{f,0} + \Omega_A \sin(2\pi f t + \phi), \tag{12}$$
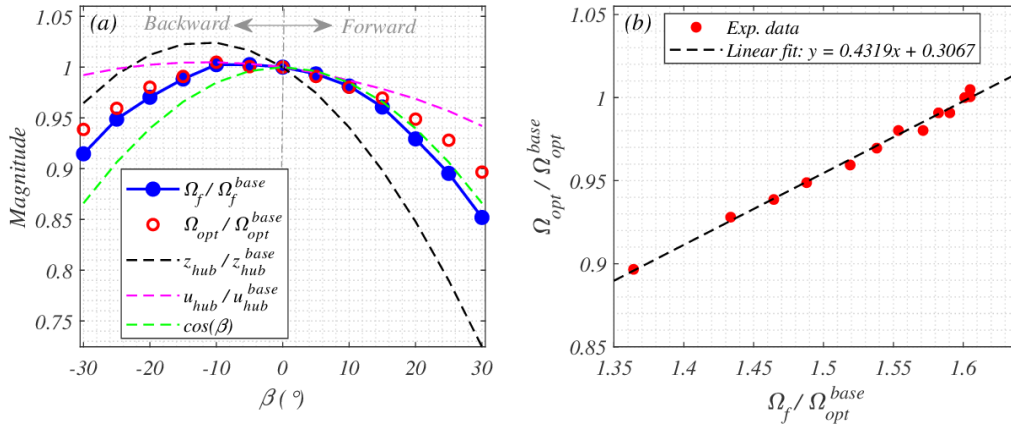
Figure 8. Fixed phase of pitch, i.e., tilt angle situation: (a) Normalized free-rotation speed, optimal rotor speed, hub height and hub-height velocity as functions of the tilt angle (β). (b) Normalized optimal rotor speed as a function of the normalized free-rotation speed. The superscript 'base' refers to quantities in the baseline case.
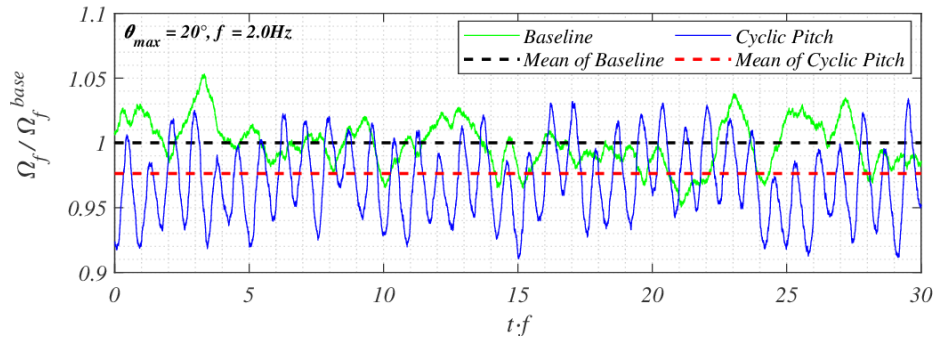
Figure 9. Time variation of the normalized free-rotation speed as a function of the normalized time ($t \cdot f$, where t is the time and f is the pitch frequency) for the cyclic pitch case with $f = 2.0Hz$ and $\theta_{max} = 20°$.

where $\Omega_{f,0} = \Omega_f(\overline{u}_{hub}, 0)$, $\Omega_A = \theta_{max}\sqrt{(2\pi fh)^2 (\partial_u \Omega_{f,0})^2 + (\partial_\theta \Omega_{f,0})^2}$ is the amplitude of variation and $\phi = \tan^{-1}(2\pi fh \partial_u \Omega_{f,\theta}/\partial_\theta \Omega_{f,0})$ is the phase shift from $\theta(t)$. Values of $\Omega_{f,0}$, Ω_A and ϕ can be quantified based on the free-rotation tests and further used to estimate the optimal rotation speed and track the maximum power points during cyclic pitch motions.

4. Conclusion

Wind tunnel experiments were performed on an in-house developed floating wind turbine model to investigate the effects of cyclic pitch motion on its power performance. Various cyclic pitch motions with different combinations of control parameters, including the pitch frequency and the pitch amplitude (i.e., the maximum pitch angle), were tested. It was found that the time variation of power production is quite periodic during cyclic pitching, especially for cases with high frequencies and amplitudes. In an atmospheric boundary layer inflow, for the ranges of pitch parameters tested with the WiRE-01 miniature wind turbine in this study, the mean power production was found to increase with the increase of pitch frequency but decrease with the increase of pitch amplitude. Power fluctuations were found to be more significant in cyclic pitch

cases than in the baseline case, as they had contributions from both flow turbulence and pitch motions. Based on the test of the free-rotation speed variation of the turbine model during cyclic pitch motion, it was found that the available power varies periodically during cyclic pitch motion. This suggests that periodic rotor speed control can be applied to maximize the power production.

In future research, dynamic rotor speed control will be applied when the turbine is in pitch motion. In addition, we will explore the effects of cyclic pitching on the wake of OFWTs and further investigate the effects on both power performance and wake characteristics of downstream turbines.

References

[1] Thiagarajan K P and Dagher H J 2014 *Journal of offshore mechanics and Arctic engineering* **136** 020903

[2] Jonkman J M 2007 *Dynamics modeling and loads analysis of an offshore floating wind turbine* (University of Colorado at Boulder)

[3] Orszaghova J, Taylor P H, Wolgamot H A, Madsen F J, Pegalajar-Jurado A M and Bredmose H 2021 *Journal of Fluid Mechanics* **929** 32

[4] Cottura L, Caradonna R, Novo R, Ghigo A, Bracco G and Mattiazzo G 2022 *Journal of Ocean Engineering and Marine Energy* **8** 319–330

[5] Koo B J, Goupee A J, Kimball R W and Lambrakos K F 2014 *Journal of Offshore Mechanics and Arctic Engineering* **136** 020907

[6] Duan G, Dar A S and Porté-Agel F 2023 *Energy Conversion and Management* **293** 117445

[7] Bastankhah M and Porté-Agel F 2017 *Energies* **10** 908

[8] Bastankhah M and Porté-Agel F 2015 A wind-tunnel investigation of wind-turbine wakes in yawed conditions *Journal of Physics: Conference Series* vol 625 p 012014

[9] Bastankhah M and Porté-Agel F 2019 *Journal of Renewable and Sustainable Energy* **11**